

# NEAR MONOCHROMATIC DUCTED GRAVITY WAVES ASSOCIATED WITH A CONVECTIVE SYSTEM CLOSE TO THE PYRENEES

Carlos Román-Cascón<sup>1</sup>, Carlos Yagüe<sup>1</sup>, Samuel Viana<sup>2</sup>, Mariano Sastre<sup>1</sup>, Gregorio Maqueda<sup>3</sup>, Marie Lothon<sup>4</sup>, Iñigo Gómara<sup>1,5</sup>

*(1) Dept. de Geofísica y Meteorología. Universidad Complutense de Madrid, Spain.*

*(2) AEMET, Spain.*

*(3) Dept. de Astrofísica y Ciencias de la Atmósfera. Universidad Complutense de Madrid, Spain.*

*(4) Université de Toulouse, Laboratoire d'Aérodynamique – CNRS UMR 5560, France.*

*(5) Instituto de Geociencias (IGEO), UCM, CSIC, Spain.*

Revision submitted to

*Q. J. R. Meteorol. Soc.*

11 June 2014

<sup>1</sup> **Correspondence to:** Carlos Román-Cascón. Dpto. Geofísica y Meteorología. Universidad Complutense de Madrid. Facultad de CC. Físicas. Avda. Complutense s/n. 28040 Madrid. Spain. E-mail: [carlosromancascon@ucm.es](mailto:carlosromancascon@ucm.es)

**Abstract (234/300 words)**

Near monochromatic gravity waves (GWs) associated with a mesoscale convective system (MCS) were detected during the Boundary Layer Late Afternoon and Sunset Turbulence (BLLAST) field campaign in Lannemezan (France) on 21 June 2011. These GWs are analysed using available instrumental data (e.g. an array of microbarometers, a microwave system Humidity And Temperature PROfiler (HATPRO) and an ultra-high frequency (UHF) wind profiler). Pressure oscillations of up to 0.5 hPa were recorded after a pronounced pressure drop of 1.4 hPa, identified as the MCS weak low. Wavelet analysis and evaluated wave parameters confirm the occurrence of such GWs (period ~ 9 minutes, horizontal wavelength ~ 7 km) which propagated from southwest to northeast, i.e. in the same direction of propagation as the MCS. Observational evidence suggests the downdrafts associated with the rear-inflow jet at the weak low zone of the MCS as the most likely generator mechanism of the GWs. However, the complex orography and proximity of the Pyrenees to the field campaign could also play an important role. Wave propagation was possible through the ducting mechanism, favoured by the existence of a critical level in a wind sheared environment around 2000 m above ground level. Wave-like motions related to the GWs passage were also observed in other atmospheric parameters close to the surface and within the lower troposphere. The GWs effects on the surface fluxes have also been analysed through Multi-Resolution Flux Decomposition (MRFD) methods.

**Keywords** – Gravity waves, wave ducting, mesoscale convective system, weak low, downdrafts, critical level, MRFD.

**Short title** – Gravity waves associated with a convective system.

## **1. Introduction**

Waves in fluids are manifested by oscillations of fluid particles moving with a slight phase difference among them and their neighbouring particles (Nappo, 2012). They are named gravity waves (GWs) when the restoring force of gravity acts to recover the equilibrium state after the destabilisation caused by some trigger mechanism (e.g. orography) in a stable stratified fluid. In the atmosphere, air parcels acquire vertical component of motion after this destabilization and tend to oscillate while trying to recover their initial state.

Although the mechanisms generating GWs are varied and complex, several triggering factors have been proposed in the literature: (i) geostrophic adjustment (e.g. Luo and Fritts, 1993), (ii) topography (e.g. Nastrom and Fritts, 1992), (iii) jet streams (e.g. Fritts and Nastrom, 1992), (iv) wind shear (e.g. Merrill and Grant, 1979), (v) katabatic flows (e.g. Viana *et al.*, 2010), (vi) convective currents (e.g. Lane and Reeder, 2001) and (vii) downdrafts (e.g. Jewett *et al.*, 2003).

When the atmospheric conditions are appropriate, the formed waves propagate towards some directions (preferably in the main wind direction); then they weaken in time and finally they transfer their energy to the main flow (Nappo, 2012) or dissipate through turbulence (Einaudi and Finnigan, 1993; Smedman *et al.*, 1995). In fact, these GWs have frequently been associated with intermittent turbulence during night-time in the Planetary Boundary Layer (PBL) (Chimonas, 1999).

With the exception of the PBL, the atmosphere is nearly always stably stratified. Therefore, GWs can frequently occur with a wide variety of characteristics (Nappo, 2012). Once the wave is formed, an additional mechanism is needed for its maintenance and propagation. In some cases, the trigger mechanism is continuous and provides enough energy to continue generating GWs, for example in cumulonimbus clouds, where convection is strong and persistent (Lindzen and Tung, 1976). In other cases, the thermal and/or dynamic profiles of the atmosphere may favour the horizontal propagation of the GWs in a layer known as wave duct. This is similar, in some way, to the use of the Scorer parameter in trapped orographically generated GWs (Mountain Waves), which has been widely used in numerous works (Doyle and Durran, 2002). Thus, a duct layer is formed for certain GWs when stratification and wind conditions (which are included in the Scorer parameter) is larger than the horizontal wavenumber of the concerned wave. The ducting mechanism was studied by Lindzen and Tung (1976) and has been identified in several observational studies (e.g. Ralph *et al.*, 1993, 1997; Monserrat and Thorpe, 1996; Doyle and Durran, 2002; Viana *et al.*, 2009).

Scientific interest in atmospheric GWs has remarkably increased during the last years (Fritts and Alexander, 2003; Nappo, 2012). On one hand, GWs are an important source of energy and momentum transport in the atmosphere and thus need an accurate parameterisation in Numerical Weather Prediction (NWP) models (Fritts and Alexander, 2003). On the other hand, GWs appear to influence the formation and evolution of convective systems (e.g. Uccellini, 1975; Balachandran, 1980; Nicholls and Pielke, 2000). In addition, GWs can also produce widespread damage due to their associated wind gusts, which represent a potential threat for aviation during landing and take-off manoeuvres (Fujita and Caracena, 1977; Manasseh and Middleton, 1995; Miller, 1999,

2000). In some cases, GWs associated with weak low zones of mesoscale convective systems (MCSs) (Fig. 1 in Houze *et al.* 1989) can also produce dangerous wind gusts at the surface in regions of the MCS where no severe winds are expected (Loehrer and Johnson, 1995; Bernardet and Cotton, 1998; Coleman and Knupp, 2009).

A wake low is a relative surface pressure minimum observed at the rear part of a MCS during its mature or dissipation stage, near the back edge of the trailing stratiform precipitation region. Together with the weak low, the thunderstorm surge and the thunderstorm high have also been identified as MCS features (Fujita, 1955; Johnson, 2001). The decrease in surface pressure associated with wake lows can be considerably important, reaching several hPa in a few minutes (Fujita, 1963; Schneider, 1990). The reasons for such quick and intense pressure drop have been discussed over years (Fujita, 1955, 1963; Pedgley, 1962; Williams, 1963; Johnson and Hamilton, 1988), and conclusions from these studies agree that the subsidence due to the descending rear-inflow jet at the rear part of MCSs causes an adiabatic warming that makes the surface pressure to decrease (Johnson and Hamilton, 1988). This pressure drop and its subsequent increase have been observed in many squall lines, bow echoes or MCSs in general (Johnson, 2001; Loehrer and Johnson, 1995). Some of these studies have related observed GWs to wake lows. For instance, Bosart and Seimon (1988) analysed a case study of an intense GW related to a squall line weak low, which caused strong fluctuations in pressure and intense wind gusts at surface. Bauck (1992) also studied large pressure drops of 3-6 hPa associated with long-distance propagating GWs, which caused important vertical displacements and intense wind gusts.

However, the presence of clear and stable oscillations in the surface pressure records over a few wave cycles associated with these weak lows has been reported less

frequently in the literature, mostly due to the lack of precise, high resolution pressure data. This work presents a singular and comprehensive observational study of near monochromatic and ducted GWs associated with the weak low of a MCS detected in a highly instrumented site near the Pyrenees. Among the measurements used, the combination of data from three high resolution microbarometers, an ultra-high frequency (UHF) wind profiler and a microwave system Humidity And Temperature PROfiler (HATPRO) radiometer has allowed us to perform a deep analysis and to offer substantiated hypotheses about the origin, propagation and effects of the GWs.

The paper is divided as follows: section 2 introduces the Boundary Layer Late Afternoon and Sunset Turbulence (BLLAST) field campaign and explains in detail the data used for the analysis. Results are provided in section 3 and the main conclusions and a short summary conclude the work.

## **2. Data and site**

Data used in this study have been obtained from different meteorological instruments deployed around the Centre for Atmospheric Research (CRA, *Centre de Recherches Atmosphériques* in French, 43° 07'N, 0° 21'E, 600 m above sea level (ASL)) site in Lannemezan (France) during the BLLAST field campaign. This site is located over the Plateau of Lannemezan, approximately 40 km away from the Pyrenees Mountains (Figure 1(a)). The BLLAST field campaign (Lothon *et al.*, 2014) was carried out from 14 June to 8 July 2011. A large amount of instrumentation was deployed over the area with the main aim of improving the knowledge of the late afternoon transition in the PBL. One of the objectives of the field campaign was to learn more about GWs that could be developed during the evening transition to the nocturnal boundary layer. Fair

weather days were preferred to analyse due to the better development of the convective boundary layer and a clear view of the evolution of the residual and stable nocturnal boundary layers later developed. However, several rainy and stormy days occurred during the field campaign, and this study focuses on one of them. Besides the instrumentation from BLLAST field campaign, additional barometers located at the surroundings of Lannemezan (*Pic du Midi* observatory and *Tarbes-Lourdes-Pyrénées* Airport (LFBT)) were used to determine the horizontal propagation and generation of the analysed GWs. The sites used to track the GWs propagation has been named from A to E according to their distance from site A (Table I and Figure 1(b)). Note that site D corresponds to the *Pic du Midi* Observatory. This astronomical and meteorological observatory is situated approximately 25 km SW from Site A at 2877 m ASL at the *Pic du Midi*, which is a sharp mountain detached some kilometres to the N from the Pyrenees massif main line of the Spanish-French border, where the highest peaks are located.

A triangular array of three high resolution PAROSCIENTIFIC microbarometers (Model 6000-16B) (Cuxart *et al.*, 2002), separated about 150 m and at 1 m above ground level (AGL) was deployed at site A in Lannemezan with the objective of studying gravity waves. The triangular configuration was used to characterize wave events by methods based on wavelet decompositions (Torrence and Compo, 1998; Terradellas *et al.*, 2001; Viana *et al.*, 2009, 2010, 2012), allowing the calculation of wave parameters (period, wavelength, phase velocity and direction of propagation). A sampling rate of 2 Hz was used, which enabled a resolution of around 0.002 hPa. As described above, surface pressure measurements from other barometers placed at different locations (sites B, C and E) were also used. Although the available resolution, accuracy and sampling rate of

these instruments were significantly lower than those for the microbarometers, they were quite useful to determine the extension and propagation of the GWs.

In order to determine the duct layer where the GWs were propagating, the vertical wavenumber ( $m$ ) (see section 3.3 and Eq. 1) was calculated using wind measurements from an UHF wind profiler and temperature measurements from HATPRO radiometer.

The UHF wind profiler, a PCL1300 UHF profiler manufactured by Degreane Horizon, is a pulsed Doppler radar working with a transmitted frequency of 1274 MHz and a peak power of 2.5 kW. This instrument worked with a good temporal resolution (3.5 – 6 minutes) and offered two modes: the low mode and the high mode. The low mode was based on a 150 m pulse length, and on 95 level gates spaced every 75 m starting at 100 m from the radar. Although the high mode offers measurements at higher levels, the low mode data were used in this study for the calculation of the vertical wavenumber ( $m$ ) due to the higher radial resolution and because the GWs detected in this work propagated mainly below 2000 m AGL. Wind profiles from UHF measurements were compared to measurements from another UHF wind profiler located 5 km apart from the former. This comparison (not shown) served as an additional quality control data. Both UHFs showed similar values but with a coherent time lag among observations, which agreed with the storm direction and speed of propagation.

The HATPRO profiling passive microwave radiometer (Löhnert *et al.*, 2009; Löhnert and Maier, 2012) is able to measure temperature and humidity with high temporal and spatial resolution. The instrument admits two different scanning modes: full troposphere and PBL profiling. Although the vertical resolution of the PBL profiling is higher, the full troposphere profiling mode has been used in this study due to the higher temporal resolution (~ 2.5 minutes). The analysis of the MCS covers the period from 2000 UTC

to 2200 UTC of 21 June 2011, while the GWs were observed from 2125 UTC to 2205 UTC. Quality control flags for HATPRO radiometer data indicated unreliable measurements for periods from 2000 UTC to 2100 UTC due to high values of liquid water path (rain), which meant that these data could not be used. Rain was weaker from 2100 UTC to 2130 UTC and the quality control flags indicated reduced quality data, which had to be used with caution. However, from 2130 UTC onwards, the data showed the highest quality level and since these data did not show appreciable differences with data from 2100 UTC to 2130 UTC, data from 2100 UTC onwards was used for the calculation of the vertical wavenumber. Nevertheless, for the analysis of temperature oscillations related to the GWs passage, only temperature fluctuations produced during the highest quality data period were taken into account.

Additional measurements from higher frequency instruments (Table II) were used to detect oscillations on other meteorological parameters, to analyse the meteorological conditions near surface and to perform Multi-Resolution Flux Decomposition (MRFD; Howell and Mahrt, 1997; Viana *et al.*, 2009) methods.

### **3. Results and discussion**

#### *3.1. Mesoscale convective system overview*

The analysed GWs were associated with a MCS which crossed the experimental area from 2000 UTC to 2200 UTC of 21 June 2011 (Figures 2 and 3). Figures 2 (a, b) show an overview of the convective activity during the afternoon over different regions over and around the Pyrenees, with several thunderstorms formed at the northern and southern sides of the mountains. Operational forecasters at the Spanish National Weather Service (AEMET) reported auspicious conditions for deep, severe and

organised convection over the northeast area of the Iberian Peninsula due to the existence of a pre-frontal unstable line. An extensive and organised convective system finally developed during the afternoon ((Figure 2(b,c) and Figure 3(a,b)) very close to the Pyrenees. These figures show a well-defined convective line of more than 150 km composed by several individual thunderstorms that crossed the Pyrenees and caused intense precipitation over different areas. This MCS moved from SW to NE while weakening (see evolution of precipitation in Figure 2) and reached Lannemezan at 2000 UTC. The rain gauge at the experimental site reported a total precipitation of 5.9 mm from 2015 UTC until 2130 UTC (Figure 6(b)), although some drizzle was also reported until 2200 UTC according to RADAR images and flag indicators of HATPRO radiometer.

Although a detailed analysis of the MCS structure and processes is beyond the scope of this study, the evolution in surface pressure observed at site A from 1945 UTC onwards (thick line, Figure 4(a)) is consistent with the following processes associated with the typical structure of MCSs and squall lines (Johnson and Hamilton, 1988 (see their Figure 25); Johnson, 2001). a) The increase in surface pressure from 1945 UTC to 2030 UTC has been identified as the thunderstorm high or mesohigh. This increase in pressure was caused by the cooling from evaporation of the rain during the former and more active part of the MCS. b) The pressure drop at 2105 UTC has been associated with the weak low at the rear part of the MCS, in a region of stratiform precipitation (Figure 2(e, f)). This decrease in pressure was a consequence of the adiabatic warming (decrease in density) caused by downdrafts associated with the descending rear-inflow jet of the storm (Johnson and Hamilton, 1988). The decrease of the rain rate at these times could also contribute to the pressure drop through the cease of the evaporation

(cooling) of the rain at these times. The commented downdrafts were in turn favoured by the cooling effect due to the precipitation evaporation at higher levels (Lindzen, 1974; Raymond, 1975; Jewett *et al.*, 2003), but since at that point there was not enough evaporative cooling to compensate the adiabatic warming caused by the downdrafts, a net warming occurred and a rapid decrease was observed in the surface pressure records.

Figure 4(a) shows surface pressure (thin line) measured at the *Pic du Midi* Observatory (site D). The fact that the surface pressure variations are not observed at site D compared to site A indicates that the main contributions were due to processes occurring below the height of the *Pic du Midi* Observatory. Nevertheless, part of the surface pressure drop due to the weak low was also slightly observed at site D at 2050 UTC. This fact indicates that the adiabatic warming could be produced not only below 2877 m ASL, but also at higher levels.

### 3.2. Gravity waves analysis

The most interesting feature of this event, from our point of view, was observed in the surface pressure records of the microbarometers (thick line, Figure 4(a)). At 2105 UTC, surface pressure from the three microbarometers showed a drop of 1.4 hPa in a few minutes followed by several fluctuations of 0.4-0.5 hPa from 2125 UTC to 2205 UTC. A 45-minutes Butterworth high pass filter has been applied to the microbarometers data to remove the synoptic tendency and the daily cycle, so that only higher frequency fluctuations in surface pressure are considered (Figure 4(b)). Figure 4(c) shows the wavelet energy per period and time unit: a clear energy increase is appreciated during the wave-like event centred in periods of around 9 minutes. It is worth mentioning that

most case studies of GWs related to convective activity described in the literature have longer periods (e.g., Lindzen, 1974; Ucellini, 1975; Alexander *et al.*, 2000) than the GWs analysed here. Subsequently, wave parameters (Table III) have been evaluated from the filtered surface pressure records using the exact location of the three microbarometers and phase differences analysis (Terradellas *et al.* 2001). This calculation has been done for the range of periods and times where the wavelet analysis showed the strongest signal, i.e. from 21.30 UTC to 21.45 UTC and for periods between 8 and 10 minutes. These parameters show a short range of values, which suggest a nearly monochromatic wave event. For the 9-minute period, they indicate a wavelength of 7 km approximately, a phase speed of around  $12.5 \text{ m s}^{-1}$  and a direction of propagation of  $50^\circ$  approximately (from SW to NE). After calculating the direction of propagation, it seems reasonable to assume that these GWs were formed somewhere SW from the microbarometers location (site A) and that propagated in the storm's moving direction. Data from several barometers located at different distances from site A have been analysed in order to track the GWs propagation. Figure 5(a) shows the filtered pressure from measurements of neighbouring barometers in Lannemezan and Figure 5(b) shows the same at further locations (see Figure 1(b) and Table I for locations). According to these data we can affirm that the wave propagated for at least 5 km (presumably more distance) and was firstly detected at site C (at the southernmost barometer in Lannemezan), which proves that the GWs propagation had a northward component of movement, in accordance with wavelet-derived parameters. Surface pressure from further locations (sites D and E) do not show apparent GWs oscillations. However, a decrease in surface pressure followed by an increase is clearly visible and could be an indicator of the passage of the weak low. This surface pressure drop was

observed at site D approximately 25 minutes before than at site A, and at site E 10-15 minutes later than at site A. According to the location of these instruments, these time lags amongst the observations agree relatively well with the speed of the storm (estimated to be  $15 \text{ m s}^{-1}$  approximately from RADAR images). It should be noted that site D corresponds to the *Pic du Midi* Observatory, situated over 2800 m ASL. Since GWs have been determined to propagate mainly below 2000 m AGL (or 2600 m ASL) (as will be shown later), this could also be one of the reasons why these wave-like motions were not observed in the surface pressure records of the barometer at site D. Moreover, the fact that the wake low was observed at site E but not the GWs oscillations suggest that not all the directions from the source area were favourable for the wave propagation.

We therefore conclude that the GWs were formed somewhere between 4 km (site C) and 25 km towards the SW direction from site A. The 25 km limit has been imposed due to the no-observation of the GWs at site D and since there are mountains higher than the top height where the wave propagation was feasible from this limit towards the SW direction. Vertical velocity measured by the UHF wind profiler (Figure 6(a)) shows a region of strong negative velocities from 2100 UTC to 2130 UTC from surface to 2500 m AGL approximately and a more specific region of even stronger vertical velocities ( $-9 \text{ m s}^{-1}$  to  $-10 \text{ m s}^{-1}$ ) around 1500 - 2500 m AGL from 2115 UTC to 2125 UTC. Although it is hard to disentangle whether the UHF vertical velocities were caused by air downdrafts, by the velocity of the rain drops or by the combination of both effects, these stronger vertical velocities do not coincide with the maximum rain rates observed at the site according to the information provided by the rain gauge (see Figure 6(b)) and RADAR images (Figure 2). Therefore, these negative vertical velocities can indicate

downdrafts regions of the MCS and, as commented before, have been related to the surface pressure drop and proposed to be responsible of the GWs initiation.

The association between GWs and weak lows has been previously documented in several studies and agrees quite well with the case study presented herein. However, it is difficult to point out whether the processes associated with the weak low zone of the MCS were the only ones involved in the GWs formation. The possible topographic effect of this mountainous area could play an important role in the final formation of the GWs. The *Pic du Midi* is the closest high mountain of the Pyrenees from Lannemezan in the SW direction, although it is detached from the main line of the highest peaks that are around the France-Spain border. Since GWs were propagated in a layer below 2000 m AGL and they were not observed at site D, we can conclude that the main mountain massif of the Pyrenees (located farther south from the *Pic du Midi*, see Figure 1) was not directly involved in the GWs formation. On the other hand, the GWs formation could have been influenced by the combination of the effects of the wake low downdrafts and the orography between *Pic du Midi* and Lannemezan, i.e.: by the lee side of the *Pic du Midi*, by lower mountains between the *Pic du Midi* and Lannemezan or even by the southern border of the Plateau of Lannemezan. However, the specific role of the mountains is very difficult to determine with the available data. Specific numerical simulations with simplified 2D and 3D models or even with NWP models could add valuable information to this point.

### 3.3. *Wave ducting*

A mechanism which favours the GWs maintenance and propagation should exist when there is not a continuous source of energy. It is known as wave ducting and occurs when

a reflecting layer at some height cause the vertical wave reflection, thus allowing the horizontal propagation of the GWs trapped between two levels in a layer known as duct layer (Lindzen and Tung 1976). According to the wave ducting theory, the properties of a wave duct can be obtained from the Taylor-Goldstein equation (Nappo, 2012):

$$\frac{d^2 w'}{dz^2} + m^2 w' = 0 \quad (1)$$

Where  $w'$  is the perturbation of the vertical velocity ( $w$ ),  $z$  is the height and  $m$  is the vertical wave number, defined by:

$$m^2 = \frac{N^2}{c_i^2} + \frac{U_{zz}}{c_i} - k_h^2 - \frac{1}{4H^2} \quad (2)$$

Here,

$$N^2 = \left( \frac{g}{\theta_0} \right) \left( \frac{\partial \theta}{\partial z} \right)$$

(3)

is the square of the Brunt-Väisälä frequency,  $c_i = c - U$  the intrinsic phase velocity ( $c$ ) relative to the mean flow ( $U$ ),  $U_{zz}$  is the second derivative with respect to height of the mean wind in the direction of propagation of the wave,  $k_h$  is the horizontal wavenumber ( $k_h = (2 \pi) / \lambda$ , where  $\lambda$  is the wavelength of the GWs) and  $H$  is a height scale of the atmosphere, sufficiently large for neglecting the fourth term on the right-hand of Eq. (2). The vertical wavenumber ( $m$ ) will show real values in regions where the horizontal propagation of the wave is favoured, and therefore, positive values of  $m^2$  will indicate a possible duct layer while negative values will indicate regions where the waves become evanescent. Hatched areas in Figure 7 indicate negative values of  $m^2$ , while non-hatched

areas denote positive values of  $m^2$ . These values have been calculated using quality-controlled temperature profiles from HATPRO radiometer, wind from UHF wind profiler and the values of wave parameters evaluated in section 3.2 for  $k_h$  and  $c$ . The phase speed of the GWs has been assumed as constant ( $c=12.5 \text{ m s}^{-1}$ ), as well as the horizontal wavenumber ( $k_h = 8.3 \times 10^{-4} \text{ m}^{-1}$ , corresponding to a wavelength of 7500 m). The direction of propagation of the GWs ( $50^\circ$ ) was used for projecting the horizontal wind in this direction. Positive values of  $m^2$  show a well-defined layer where the wave propagation was possible, determined by an intense wind shear existent above 2000 m AGL approximately (Figure 7), which served as an effective reflecting layer with a critical or steering level, i.e. a level wherein the wind speed of the main flow equals the phase speed of the GWs (Lindzen and Tung (1976)). In this case, the bottom layer of the wave duct was the ground.

Calculated values of  $m^2$  are positive for the whole available vertical profile also before the arrival of the pressure drop or weak low and prior to the record of the wave-like motions in surface pressure, however, it was just after the arrival of this weak low (after 2115 UTC) when the GWs were detected, coinciding with a confinement of the duct layer (where  $m^2$  shows positive values) in the lowest atmospheric levels. Figure 7 also shows the horizontal wind speed for the event and it proves that the duct layer defined between surface and approximately 2000 m AGL was mainly determined by the wind profile, with an intense wind shear existent at the rear part of the MCS, just behind the wake low.

On the other hand, a further exploration of the filtered pressure records and wavelet analysis (Figure 4(b,c)) shows a temporary decrease in the period (from 9 to 6 minutes) of the wave-like disturbances at 2145 UTC, which coincides with a narrowing of the

duct layer where the wave was able to travel (Figure 7). This narrowing was in turn conditioned by the position of the critical level found around 2000 m AGL, which temporarily descended from 2000 to 1800 m AGL approximately. This coincidence suggests that the thickness of the duct layer could have influenced the frequency of the concerned GWs.

#### *3.4. GWs effects close to the surface and in the lower troposphere*

GWs perturb the environment where they propagate and cause oscillations in other meteorological parameters besides surface pressure. The relative phases and amplitudes of these parameters are described by polarization equations from the linear wave theory (see for example Fritts and Alexander, 2003; Nappo, 2012). In this case study, temperature and humidity oscillations associated with the passage of the GWs were observed in the lower troposphere (Figure 8). A certain phase lag is observed between these oscillations and surface pressure fluctuations, in agreement with the expected  $\pi/2$  phase relationship from the linear wave theory. However, due to the non-perfect monochromaticity of the GWs and the low time resolution of the HATPRO radiometer measurements, it is difficult to assess how closely this polarization relation is fulfilled.

The observed oscillations suggest propose that the air parcels were vertically narrowed (maxima of pressure) and spread (minima of pressure) alternatively by the action of the GWs. The vertical narrowing of the layer caused displacements of upper air parcels (colder and with higher relative humidity) to lower layers and the spreading associated with minima of surface pressure caused the contrary. Near saturation values of relative humidity indicate approximately the position of the cloud base; the oscillations detected

in these records (around 3500 m AGL) suggest that the GWs could shape and produce a wave-like cloud base. The effect of the GWs was also noted in wind measurements below 2000 m AGL: this layer was characterized by light winds and slight and alternating changes in wind direction (not shown).

Higher frequency data from instruments at site A were used to check whether the oscillations in these meteorological parameters were also encountered near surface. A combination of cooling produced by the evaporation of the rain water at the surface and radiative cooling during sunset most likely caused the formation of a surface-based temperature inversion from 2000 UTC onwards (Figure 9). Later, the arrival of the GWs to the site caused oscillations in wind speed, wind direction, temperature and vertical velocity measurements at different heights close to the surface. Figure 10 shows examples of the relationships found among surface pressure and other surface parameters at 45 m: (a) wind speed projected in the same direction of propagation of the GWs (50°), (b) wind direction, (c) temperature and (d) vertical velocity perturbation (Eq. 3), where the mean of the vertical velocity has been calculated from 2115 UTC to 2200 UTC.

$$w' = w - \bar{w}$$

(3)

The observed oscillations in the wind speed projected in the same direction than the GWs have the same periodicity than the surface pressure records. This suggests that the effect of the GWs during narrowings (maxima in pressure) was to force the main flow to approach their own direction of propagation, as can be also seen in the changes in

wind direction (closer to southwest during maxima). This relation between wind and pressure can be obtained from the polarization equations (Nappo, 2012):

Where  $c$  is...,  $\rho$ ....

It can be seen that if  $c$  is larger than wind  $u$  and  $p$  are in phase as it has been found for our data. This relationship was also found in Viana et al. (2009).

Although some temperature oscillations near to the surface seem also to be related to the GWs effect (Figure 10c), these oscillations are more difficult to study further, since they are also affected by small changes in wind direction (local advection) in a highly heterogeneous terrain and not only by the vertical narrowing/spreading of the layer affected by GWs. Finally, changes in the perturbation of the vertical velocity measured by a sonic anemometer at 45 m are also observed, as seen in other studies (Viana et al. 2009; Birch et al. 2013). Maxima in pressure correspond to minima in the vertical velocity measurements and vice versa.

Surface pressure records and oscillations observed in these parameters at other heights have also been compared (not shown), and in some cases they show similar agreements than for 45 m measurements. Although some of these relations agree qualitatively well with the phase relationships obtained from the polarization equations (mainly the phase between pressure and wind), other phase relationships are not achieved, in accordance with the results obtained in Viana et al. (2009). As Nappo (2012) pointed out, turbulence in the surface layer affects wave perturbations, and although for simplicity, linear theory is applied to these waves, gravity waves in the planetary boundary layer are seldom linear (Finnigan, 1988) and consequently the theoretical phase relationships are difficult

to observe. Anyway, a detailed analysis of the linear polarization equations is out of the scope of this study and difficult to perform in the real atmosphere.

In addition, MRFD analysis has been applied to high-frequency data from a sonic anemometer located at 2 m AGL in order to study the effects caused by the propagation of the GWs on the surface fluxes. The MRFD method (Howell and Mahrt, 1997) is applied when attempting to distinguish the contribution of the different temporal scales to the fluxes and it usually allows separating turbulence from larger-scale contributions to the fluxes, such as gravity waves. Each vertical section of these figures shows the MRFD analysis performed every 60 s, using time series of 820 s and gradually dividing these time series until time series of 0.1 s. A running mean of 5 minutes has been applied to the MRFD results for smoothing. High values of friction velocity are observed in Figure 11 (a) until 2045 UTC, due to relatively high winds associated with the passage of the more active part of the MCS, with important contributions of scales between 1 s and 300 s (turbulent). Afterwards, the turbulence decays significantly as a consequence of the decrease in wind speed and the stabilization of the layer. The formed surface based thermal inversion caused an increase in the vertical heat flux (Figure 11 (b)) around 2130 UTC. Although the turbulence remained relatively weak during the GWs propagation over the site, it increased with the GWs arrival at 2120 UTC, probably due to the effect of the GWs generating turbulence by non linear effects and the oscillations in wind speed.

In addition, an increase in the contribution to the friction velocity and heat flux occurred for temporal scales larger than 300 s during the wave event. These temporal scales coincide with the order of magnitude of the calculated period of the GWs (around 9 minutes). It should also be noted the positive values encountered for the vertical heat

flux observed during the wave event, frequently known as counter-gradient fluxes when they are found in stable environments, since they indicate an upward heat flux. Counter-gradient fluxes have been associated with wave breaking activity during stable conditions in the PBL (Nai-Ping *et al.*, 1983; Yagüe and Redondo, 1995; Chimonas, 1999). In this case, these counter-gradient fluxes from higher temporal scales coincided with the GWs and coexisted with the co-gradient (positive vertical heat fluxes) turbulent heat fluxes from lower temporal scales.

#### **4. SUMMARY AND CONCLUSIONS**

Near monochromatic GWs associated with a MCS were detected on 21 June 2011 during the BLLAST field campaign in Lannemezan (France). These GWs have been analysed in detail taking advantage of the large amount of available data. The clearest manifestation of these GWs was observed in the surface pressure records measured by an array of three high resolution microbarometers, showing clear sinusoidal oscillations of 0.4-0.5 hPa. Wavelet analysis has been performed and wave parameters have been evaluated, suggesting the occurrence of GWs propagating from SW to NE with around 9 minutes of period, a wavelength of 7 km and, a phase speed of around 12.5 m s<sup>-1</sup>. These wave-like motions were preceded by a surface pressure drop of 1.4 hPa, which has been identified as the weak low of the MCS. The location of the pressure drop at the rear part of the MCS, the negative values of vertical velocity measured by the UHF wind profiler and the resemblance to the structure of many other documented MCSs support this weak low hypothesis.

The downdrafts related to the wake low have been proposed to be the most likely mechanism responsible of the GWs initiation in a stable stratified atmosphere. GWs

tracking was performed with additional barometers placed at different locations and showed that not all the directions were favourable for the wave propagation. Although the orography between the *Pic du Midi* and Lannemezan could have played an important role in the final formation of the GWs, this effect could not be further analysed due to the lack of measurements between the *Pic du Midi* and Lannemezan. The propagation of the GWs in the SW-NE direction was favoured by the existence of a duct layer defined by positive values of  $m^2$  (vertical wavenumber) between surface and 2000 m AGL. The thickness of the duct layer was mainly determined by the wind profile, characterized by a wind sheared zone with a critical level around 2000 m AGL. This critical level caused the vertical reflection of the GWs and permitted their horizontal propagation. The uncommon properties of these GWs compared to those usually associated with convection seemed to be possible in part by the relatively low position of the wind shear and the critical level, i.e. these observations suggest some proportionality between the position of the critical level and the dimensions and properties of the GWs.

The GWs effects were also observed in the wind, temperature and humidity time series close to the surface and within the lower troposphere. The contributions of the different temporal scales to the surface fluxes (evaluated through MRFD analyses) were also affected by the GWs passage, which produced an increase in turbulence at certain moments, important contribution to the fluxes from larger temporal scales and counter-gradient fluxes.

Although a detailed analysis was possible in this study, some questions still remain open, especially those concerning the GWs origin and the role of the orography. Numerical simulations and the observational analysis of similar case studies at this site

as well as at other locations not affected by mountains would add valuable information to these unresolved questions.

## **ACKNOWLEDGMENTS**

This research has been funded by the Spanish Government (projects *CGL2009-12797-C03-03*, *CGL2011-13477-E* and *CGL2012-37416-C04-02*). BLLAST field experiment was made possible thanks to the contribution of several institutions and supports: INSU-CNRS (*Institut National des Sciences de l'Univers*, *Centre national de la Recherche Scientifique*, LEFE-IDAO program), Météo-France, *Observatoire Midi-Pyrénées* (University of Toulouse), EUFAR (European Facility for Airborne Research) and COST ES0802 (European Cooperation in the field of Scientific and Technical). The field experiment would not have occurred without the contribution of all participating European and American research groups, which all have contributed in a significant amount. BLLAST field experiment was hosted by the instrumented site of *Centre de Recherches Atmosphériques*, Lannemezan, France (*Observatoire Midi-Pyrénées*, *Laboratoire d'Aérodologie*). BLLAST data are managed by SEDOO, from *Observatoire Midi-Pyrénées*. The tower equipment and UHF radar have been supported by CNRS, University of Toulouse and European POCTEFA FluxPyr program and FEDER program (Contract 34172 – IRENEA – ESPOIR). Corn and Moor stations were funded by the CNRS INSU and Météo-France and implemented by the CNRM-GAME team GMEI/4M. We thank François Gheusi and Gilles Athier for providing data from the *Pic du Midi* station -- part of the P2OA research platform. These measurements have been supported by the French national institute CNRS-INSU and the *Observatoire Midi-Pyrénées* (University of Toulouse). The edge-site measurements were financed by the

DFG (Deutsche Forschungsgemeinschaft) project GR2687/3-1 and SCHU2350/2-1; Links between local-scale measurements and catchment-scale measurements and modeling of gas exchange processes over land surfaces. Thanks to Satellite Receiving Station from Dundee University for providing a high resolution satellite image, to Jesús González Gálvez for helpful communication about HATPRO radiometry and to Larry Mahrt for his comments. Finally, the authors would like to thank the two anonymous reviewers for their helpful comments.

## REFERENCES

Alexander MJ, Beres JH, Pfister L. 2000. Tropical stratospheric gravity wave activity and relationships to clouds. *J. Geophys. Res.* **105** : 22299 - 22309. DOI:

10.1029/2000JD900326.

Balachandran NK. 1980. Gravity waves from thunderstorms. *Mon. Wea. Rev.* **108** : 804 - 816. DOI: [http://dx.doi.org/10.1175/1520-0493\(1980\)108<0804:GWFT>2.0.CO;2](http://dx.doi.org/10.1175/1520-0493(1980)108<0804:GWFT>2.0.CO;2)

Bauck BH. 1992. An unusually strong gravity wave over western Washington. *Wea. Forecasting.* **7** : 389 - 397. DOI: [http://dx.doi.org/](http://dx.doi.org/10.1175/1520-0434(1992)007<0389:AUSGWO>2.0.CO;2)

10.1175/1520-0434(1992)007<0389:AUSGWO>2.0.CO;2

Bernardet LG, Cotton WR. 1998. Multiscale evolution of a derecho-producing mesoscale convective system. *Mon. Wea. Rev.* **126** : 2991 – 3015. DOI: [http://dx.doi.org/10.1175/1520-0493\(1998\)126<2991:MEOADP>2.0.CO;2](http://dx.doi.org/10.1175/1520-0493(1998)126<2991:MEOADP>2.0.CO;2)

Birch CE, Parker DJ, O'Leary A, Marsham JH, Taylor CM, Harris PP and Lister GMS. 2013. Impact of soil moisture and convectively generated waves on the initiation of a West African mesoscale convective system. *Q.J.R. Meteorol. Soc.* **139**: 1712–1730. doi: 10.1002/qj.2062

Bosart LF, Seimon A. 1988. A case study of an unusually intense atmospheric gravity wave. *Mon. Wea. Rev.* **116** : 1857 - 1886. DOI: [http://dx.doi.org/10.1175/1520-0493\(1988\)116<1857:ACSOAU>2.0.CO;2](http://dx.doi.org/10.1175/1520-0493(1988)116<1857:ACSOAU>2.0.CO;2)

Chimonas G. 1999. Steps, waves and turbulence in the stably stratified planetary boundary layer. *Boundary-Layer Meteorol.* **90** : 397 – 421. DOI: 10.1023/A:1001709029773

Clarke RH. 1962. Pressure oscillations and fallout downdraughts. *Q. J. R. Meteorol. Soc.* **88** : 459 – 469.

Coleman TA, Knupp KR. 2009. Factors Affecting Surface Wind Speeds in Gravity Waves and Wake Lows. *Wea. Forecasting.* **24** : 1664 – 1679. DOI: <http://dx.doi.org/10.1175/2009WAF2222248.1>

Cuxart J, Morales G, Terradellas E, Yagüe C. 2002. Study of coherent structures and estimation of the pressure transport terms for the nocturnal stable boundary layer. *Boundary-Layer Meteorol.* **105** : 305 - 328. DOI: 10.1023/A:1019974021434

Doyle JD, Durran DR, 2002. The Dynamics of Mountain-Wave-Induced Rotors. *J. Atmos. Sci.* **59** : 186 – 201. doi: [http://dx.doi.org/10.1175/1520-0469\(2002\)059<0186:TDOMWI>2.0.CO;2](http://dx.doi.org/10.1175/1520-0469(2002)059<0186:TDOMWI>2.0.CO;2)

Einaudi F, Finnigan JJ. 1993. Wave–turbulence dynamics in the stably stratified boundary layer. *J. Atmos. Sci.* **50** : 1841 – 1864. DOI: [http://dx.doi.org/10.1175/1520-0469\(1993\)050<1841:WTDITS>2.0.CO;2](http://dx.doi.org/10.1175/1520-0469(1993)050<1841:WTDITS>2.0.CO;2)

Fritts DC, Nastrom GD. 1992. Sources of mesoscale variability of gravity waves. Part II: Frontal, convective, and jet stream excitation. *J. Atmos. Sci.* **49** : 111 – 127. DOI: [http://dx.doi.org/10.1175/1520-0469\(1992\)049<0111:SOMVOG>2.0.CO;2](http://dx.doi.org/10.1175/1520-0469(1992)049<0111:SOMVOG>2.0.CO;2)

Fritts DC, Alexander MJ. 2003. Gravity wave dynamics and effects in the middle atmosphere. *Rev. Geophys.* **41** : 1003 - 1063. DOI: [10.1029/2001RG000106](http://dx.doi.org/10.1029/2001RG000106)

Fujita TT. 1955. Results of detailed synoptic studies of squall lines. *Tellus.* **7**: 405 – 436. DOI: [10.1111/j.2153-3490.1955.tb01181.x](http://dx.doi.org/10.1111/j.2153-3490.1955.tb01181.x)

Fujita TT. 1963. Analytical mesometeorology: A review. *Severe Local Storms, Meteor. Monogr.*, No. 27. Amer. Meteor. Soc. 77 – 125.

Fujita TT, Caracena F. 1977. An analysis of three weather-related aircraft accidents. *Bull. Amer. Meteor. Soc.* **58** : 1164 – 1181. DOI: [http://dx.doi.org/10.1175/1520-0477\(1977\)058<1164:AAOTWR>2.0.CO;2](http://dx.doi.org/10.1175/1520-0477(1977)058<1164:AAOTWR>2.0.CO;2)

Houze RA, Biggerstaff MI, Rutledge SA, Smull BF. 1989. Interpretation of Doppler weather radar displays of midlatitude mesoscale convective systems. *Bull. Amer. Meteor. Soc.* **70** : 608 – 619. DOI: [http://dx.doi.org/10.1175/1520-0477\(1989\)070<0608:IODWRD>2.0.CO;2](http://dx.doi.org/10.1175/1520-0477(1989)070<0608:IODWRD>2.0.CO;2)

Jewett BF, Ramamurthy MK, Rauber RM. 2003. Origin, evolution, and finescale structure of the St. Valentine's day mesoscale gravity wave observed during STORM-FEST. Part III: gravity wave genesis and the role of evaporation. *Mon. Wea. Rev.* **131** : 617 – 633. DOI: [http://dx.doi.org/10.1175/1520-0493\(2003\)131<0617:OEAFSO>2.0.CO;2](http://dx.doi.org/10.1175/1520-0493(2003)131<0617:OEAFSO>2.0.CO;2)

Johnson RH. 2001. Surface mesohighs and mesolows. *Bull. Amer. Meteor. Soc.* **82** : 13 – 31. DOI: [http://dx.doi.org/10.1175/1520-0477\(2001\)082<0013:SMAM>2.3.CO;2](http://dx.doi.org/10.1175/1520-0477(2001)082<0013:SMAM>2.3.CO;2)

Johnson RH, Hamilton PJ. 1988. The relationship of surface pressure features to the precipitation and airflow structure of an intense midlatitude squall line. *Mon. Wea. Rev.* **116** : 1444 – 1472. DOI: [http://dx.doi.org/10.1175/1520-0493\(1988\)116<1444:TROSPF>2.0.CO;2](http://dx.doi.org/10.1175/1520-0493(1988)116<1444:TROSPF>2.0.CO;2)

Lane TP, Reeder MJ. 2001. Convectively generated gravity waves and their effect on the cloud environment. *J. Atmos. Sci.* **58** : 2427 – 2440. DOI: [http://dx.doi.org/10.1175/1520-0469\(2001\)058<2427:CGGWAT>2.0.CO;2](http://dx.doi.org/10.1175/1520-0469(2001)058<2427:CGGWAT>2.0.CO;2)

Lindzen RS. 1974. Wave-CISK in the tropics. *J. Atmos. Sci.* **31** : 156 – 179. DOI: [http://dx.doi.org/10.1175/1520-0469\(1974\)031<0156:WCITT>2.0.CO;2](http://dx.doi.org/10.1175/1520-0469(1974)031<0156:WCITT>2.0.CO;2)

Lindzen RS, Tung K-K. 1976. Banded convective activity and ducted gravity waves. *Mon. Wea. Rev.* **104**: 1602 - 1617. DOI: [http://dx.doi.org/10.1175/1520-0493\(1976\)104<1602:BCAADG>2.0.CO;2](http://dx.doi.org/10.1175/1520-0493(1976)104<1602:BCAADG>2.0.CO;2)

Loehrer SM, Johnson RH. 1995. Surface pressure and precipitation life cycle characteristics of PRE-STORM mesoscale convective systems. *Mon. Wea. Rev.* **123** : 600 – 621. DOI: [10.1175/1520-0493\(1995\)123<0600:PSPLC>2.0.CO;2](http://dx.doi.org/10.1175/1520-0493(1995)123<0600:PSPLC>2.0.CO;2)

Löhnert U, Maier O. 2012. Operational profiling of temperature using ground-based microwave radiometry at Payerne: prospects and challenges. *Atmos. Meas. Tech.* **5** : 1121 – 1134. DOI: [10.5194/amt-5-1121-2012](http://dx.doi.org/10.5194/amt-5-1121-2012)

Löhnert U, Turner DD, Crewell S. 2009. Ground-Based Temperature and Humidity Profiling Using Spectral Infrared and Microwave Observations. Part I: Simulated Retrieval Performance in Clear-Sky Conditions. *J. Appl. Meteor. Climatol.* **48** : 1017 – 1032. DOI: [10.1175/2008JAMC2060.1](http://dx.doi.org/10.1175/2008JAMC2060.1)

Lothon M, Lohou F, Pino D, Couvreur F, Pardyjak ER, Reuder J, Vilà-Guerau de Arellano J, Durand P, Hartogensis O, Legain D, Augustin P, Gioli B, Faloon I, Yagüe C, Alexander DC, Angevine WM, Bargain E, Barrié J, Bazile E, Bezombes Y, Blay-Carreras E, van de Boer A, Boichard JL, Bourdon A, Butet A, Campistron B, de Coster O, Cuxart J, Dabas A, Darbieu C, Deboudt K, Delbarre H, Derrien S, Flament P, Fourmentin M, Garai A, Gibert F, Graf A, Groebner J, Guichard F, Jiménez-Cortés MA, Jonassen M, van den Kroonenberg A, Lenschow DH, Magliulo V, Martin S, Martínez D, Mastrorillo L, Moene AF, Molinos F, Moulin E, Pietersen HP, Piguet B, Pique E, Román-Cascón C, Rufin-Soler C, Saïd F, Sastre-Marugán M, Seity Y, Steeneveld GJ, Toscano P, Traullé O, Tzanos D, Wacker S, Wildmann N, Zaldei A. 2014. The BLLAST field experiment: Boundary-Layer Late Afternoon and Sunset Turbulence. *Atmos. Chem. Phys. Discuss.*, **14** : 10789–10852 doi: 10.5194/acpd-14-10789-2014.

Luo Z, Fritts DC. 1993. Gravity-wave excitation by geostrophic adjustment of the jet stream. Part II: Three-dimensional forcing. *J. Atmos. Sci.* **50** : 104 - 115.

DOI: [http://dx.doi.org/10.1175/1520-0469\(1993\)050<0104:GWEBGA>2.0.CO;2](http://dx.doi.org/10.1175/1520-0469(1993)050<0104:GWEBGA>2.0.CO;2).

Manasseh R, Middleton JH. 1995. Boundary layer oscillations from thunderstorms at Sydney airport. *Mon. Wea. Rev.* **123** : 1166 - 1177.

Miller DW. 1999. `Thunderstorm induced gravity waves as a potential hazard to commercial aircraft`. In *American Meteorological Society 79th annual conference. Wyndham Anatole Hotel, Dallas, TX, 10-15 Jan 1999*. American Meteorological Society.

Miller DW. 2000. `Exploring the possibility of a low altitude gravity wave encounter as the cause of a general aviation accident near Norman Oklahoma on December 6, 1998`. In *Ninth Conference on Aviation, Range, and Aerospace Meteorology. 20th Conference*

*on Severe Local Storms. Radisson Twin Towers Hotel, Orlando, Florida, 11-15 Sept 2000.* American Meteorological Society.

Monserrat S, Thorpe AJ. 1996. Use of ducting theory in an observed case of gravity waves. *J. Atmos. Sci.* **53** : 1724 - 1736. DOI: [http://dx.doi.org/10.1175/1520-0469\(1996\)053<1724:UODTIA>2.0.CO;2](http://dx.doi.org/10.1175/1520-0469(1996)053<1724:UODTIA>2.0.CO;2)

Nai-Ping L, Neff WD, Kaimal JC. 1983. Wave and turbulence structure in a disturbed nocturnal inversion. *Boundary-Layer Meteorol.* **26**: 141 - 155.

Nappo CJ. 2012. *An introduction to atmospheric gravity waves* (2<sup>nd</sup> edition). Academic Press: London.

Nastrom GD, Fritts DC. 1992. Sources of mesoscale variability of gravity waves. Part I: Topographic excitation. *J. Atmos. Sci.* **49** : 101 - 110.

DOI: [http://dx.doi.org/10.1175/1520-0469\(1992\)049<0101:SOMVOG>2.0.CO;2](http://dx.doi.org/10.1175/1520-0469(1992)049<0101:SOMVOG>2.0.CO;2)

Nicholls ME, Pielke RA. 2000. Thermally induced compression waves and gravity waves generated by convective storms. *J. Atmos. Sci.* **57** : 3251 – 3271. DOI: [http://dx.doi.org/10.1175/1520-0469\(2000\)057<3251:TICWAG>2.0.CO;2](http://dx.doi.org/10.1175/1520-0469(2000)057<3251:TICWAG>2.0.CO;2)

Pedgley DE. 1962. *A meso-synoptic analysis of the thunderstorms on 28 August 1958.* Geophysical Memo. 106, British Meteorological Office, 74 pp.

Ralph FM, Venkateswaran V, Crochet M. 1993. Observations of a mesoscale ducted gravity wave. *J. Atmos. Sci.* **50** : 3277 – 3291. DOI: [http://dx.doi.org/10.1175/1520-0469\(1993\)050<3277:OOAMDG>2.0.CO;2](http://dx.doi.org/10.1175/1520-0469(1993)050<3277:OOAMDG>2.0.CO;2)

Ralph FM, Paul JN, Teddie LK, Levinson D, Fedor L, 1997: Observations, Simulations, and Analysis of Nonstationary Trapped Lee Waves. *J. Atmos. Sci.* **54** : 1308 – 1333. doi: [http://dx.doi.org/10.1175/1520-0469\(1997\)054<1308:OSAAON>2.0.CO;2](http://dx.doi.org/10.1175/1520-0469(1997)054<1308:OSAAON>2.0.CO;2)

Raymond DJ. 1975. A model for predicting the movement of continuously propagating convective storms. *J. Atmos. Sci.* **32** : 1308 – 1317. DOI: <http://dx.doi.org/>

10.1175/1520-0469(1975)032<1308:AMFPTM>2.0.CO;2

Schneider RS. 1990. Large-amplitude gravity wave disturbances within the intense Midwest extratropical cyclone of 15 December 1987. *Wea. Forecasting.* **5** : 533 – 558.

DOI: [http://dx.doi.org/10.1175/1520-0434\(1990\)005<0533:LAMWDW>2.0.CO;2](http://dx.doi.org/10.1175/1520-0434(1990)005<0533:LAMWDW>2.0.CO;2)

Schultz DM, Kanak KM, Straka JM, Trapp RJ, Gordon BA, Zrnic DS, Bryan GH, Durant AJ, Garrett TJ, Klein PM, Lilly DK. 2006. The Mysteries of Mammatus Clouds: Observations and Formation Mechanisms. *J. Atmos. Sci.* **63** : 2409 – 2435. DOI: <http://dx.doi.org/10.1175/JAS3758.1>

Smedman A-S, Bergström H, Högström U. 1995. Spectra, variances and length scales in a marine stable boundary layer dominated by a low level jet. *Boundary-Layer Meteorol.* **76** : 211 – 232. DOI: [10.1007/BF00709352](http://dx.doi.org/10.1007/BF00709352)

Terradellas E, Morales G, Cuxart J, Yagüe C. 2001. Wavelet methods: application to the study of the stable atmospheric boundary layer under non-stationary conditions. *Dyn Atmos. Oceans.* **34** : 225 – 244.

Torrence C, Compo GP. 1998. A practical guide to wavelet analysis. *Bull Amer Meteorol Soc.* **79** : 61 – 78. DOI: <http://dx.doi.org/>

10.1175/1520-0477(1998)079<0061:APGTWA>2.0.CO;2

Uccellini LW. 1975. A case study of apparent gravity wave initiation of severe convective storms. *Mon. Wea. Rev.* **103** : 497 – 513. DOI: <http://dx.doi.org/>

10.1175/1520-0493(1975)103<0497:ACSOAG>2.0.CO;2

Viana S, Yagüe C, Maqueda G. 2009. Propagation and effects of a mesoscale gravity-wave over a weakly-stratified stable boundary layer during SABLES2006 field

campaign. *Boundary-Layer Meteorol.* **133** : 165 – 188. DOI: 10.1007/

s10546-009-9420-4

Viana S, Terradellas E, Yagüe C. 2010. Analysis of gravity waves generated at the top of a drainage flow. *J. Atmos. Sci.* **67** : 3949 – 3966. DOI: [http://dx.doi.org/](http://dx.doi.org/10.1175/2010JAS3508.1)

10.1175/2010JAS3508.1

Viana S, Yagüe C, Maqueda G. 2012. Vertical structure of the stable boundary layer detected by RASS-SODAR and in-situ measurements in the SABLES 2006 field campaign. *Acta Geophys.* **60** : 1261 – 1286.

Williams DT. 1963. *The thunderstorm wake of May 4, 1961*. National Severe Storms Project Rep. 18, U.S. Dept. of Commerce, Washington DC, 23 pp. [NTIS PB-168223].

Winstead NS, Verlinde J, Arthur ST, Jaskiewicz F, Jensen M, Miles N, Nicosia D. 2001. High-resolution airborne radar observations of mammatus. *Mon. Wea. Rev.* **129** : 159 – 166. DOI: [http://dx.doi.org/10.1175/1520-0493\(2001\)129<0159:HRAROO>2.0.CO;2](http://dx.doi.org/10.1175/1520-0493(2001)129<0159:HRAROO>2.0.CO;2)

Yagüe C, Redondo, JM. 1995. A case study of turbulent parameters during the antarctic winter. *Antarc. Sci.* **7**: 421 - 433.

## Tables

**Table I.** Information about sites of barometers used to track the GWs propagation.

<b>Site</b>	<b>Original site</b>	<b>Location</b>	<b>Distance and direction from Site A</b>	<b>Time resolution / resolution</b>
<b>Site A</b>	Microbarometer A BLLAST	43° 07' 25.5'' N 00° 21' 47.9'' E	Reference site	0.5 s / 0.002 hPa
<b>Site B</b>	Edge site BLLAST	43° 07' 53.4'' N 00° 21' 35.2'' E	1 km NNW	0.05 s (av 10 s) / 0.0001 hPa (LICOR)
<b>Site C</b>	Moor site BLLAST	43° 05' 24.5'' N 00° 21' 42.6'' E	4 km S	10 s (av 1 min) / 0.01 hPa
<b>Site D</b>	<i>Pic du Midi</i> Obs.	42° 56' 07.6'' N 00° 08' 24.2'' E	25 km SW	1 min / 0.1 hPa
<b>Site E</b>	LFBT Airport	43° 10' 59.7'' N 00° 00' 06.1'' W	30 km WNW	1 min / 0.1 hPa

**Table II.** Information about additional instruments located close to the surface.

<b>Instrument</b>	<b>Model</b>	<b>Height (AGL)</b>	<b>Freq.</b>
-------------------	--------------	---------------------	--------------

Thermometers	- <i>Campbell HMP45 thermo-hygrometers</i>	2, 15, 30, 45, 60 m	0.1 Hz
Anemometers	- <i>Wind monitor Young 05103</i>	15 m	0.1 Hz
	- <i>Vector Instrument W2009 wind vane</i>	45 m	0.1 Hz
Sonic anemometers	- <i>Campbell Csat3 3D</i>	45 m	10 Hz
	- <i>METEK USA 1 - (used for MRFD)</i>	2 m	20 Hz

**Table III.** Wave parameters calculated from wavelet analysis.

Wave parameter	Range of values from 2130 UTC to 2145 UTC
----------------	---

---

<b>Period</b>	[7 – 11] min
<b>Wavelength</b>	[6500 – 8000] m
<b>Phase speed</b>	[12 – 14] m s <sup>-1</sup>
<b>Direction of propagation</b>	[45 – 60] °

---

**Figure captions.**

**Figure 1.** a) Geographical location of the BLLAST field campaign site (Lannemezan) and surroundings. Land topography given in light-green to dark-red shadings (in meters). (b) Zoomed area (dashed rectangle from (a)) with locations of barometer sites used to track the GWs propagation. Source: The Global Land One-km Base Elevation Project (GLOBE).

**Figure 2.** RADAR composites of cumulative precipitation (mm) over the 15 minutes preceding each hour between 1700 UTC and 2200 UTC (a to e). Sites A and D are marked with black points.

**Figure 3.** Satellite images at (a) 1800 UTC, (b) 1900 UTC and (c) 2000 UTC on 21 June 2011. Figures a and b from visible satellite images of Meteosat RGB Segment 5. Figure c from AVHRR Channel 4 (thermal) of NOAA 16 satellite (Copyright NERC Satellite Receiving Station, Dundee University, Scotland, <http://www.sat.dundee.ac.uk>).

**Figure 4.** a) Surface pressure (hPa) measured by microbarometer A in Lannemezan (Site A, thick line) and by the barometer (+225 hPa) at the *Pic du Midi* Observatory (Site D, thin line) for 21 June 2011. b) Microbarometer A filtered pressure (hPa). c) Wavelet energy density per period and time unit ( $\text{hPa}^2 \text{s}^{-1}$ ).

**Figure 5.** a) Filtered surface pressure (hPa) at nearby locations in Lannemezan: site A (red thin line), site B (blue dashed line) and site C (black thick line). b) Idem for further locations: site D (blue thin line) and site E (black thick line).

**Figure 6.** a) Vertical velocity ( $\text{m s}^{-1}$ ) measured by the UHF wind profiler at site A. Surface pressure time series from microbarometer A is overlaid for reference (black line). b) Rain measured at site A (mm).

**Figure 7.** Wind speed ( $\text{m s}^{-1}$ ) measured by the UHF wind profiler at site A. Hatched areas indicate negative  $m^2$  values, while non-hatched areas indicate positive  $m^2$  values, marking the duct layer. Surface pressure time series from microbarometer A is overlaid for reference (red line).

**Figure 8.** (a) Temperature (K) and (b) relative humidity (%) measured by HATPRO radiometer. Surface pressure time series from microbarometer A is overlaid for reference (black line).

**Figure 9.** Potential temperature profiles from 60m tower measurements at different times (2000 UTC, solid black line; 2015 UTC, dashed blue line; 2030 UTC, dotted red line; 2045 UTC, dashed-dotted green line).

**Figure 10.** Time series of meteorological parameters at 45 m (dashed black line) and surface pressure (solid blue line) during the GWs event. a) Wind speed projected in the same direction of GWs propagation ( $\text{m s}^{-1}$ ). b) Wind direction ( $^\circ$ ). c) Temperature ( $^\circ\text{C}$ ). d) Vertical velocity perturbation ( $\text{m s}^{-1}$ )

**Figure 11.** Multi-Resolution Flux Decomposition (MRFD) of (a) friction velocity ( $\text{m s}^{-1}$ ) and (b) heat flux ( $\text{K m s}^{-1}$ ) at 2 m AGL. Surface pressure time series from microbarometer A is overlaid for reference (black line).



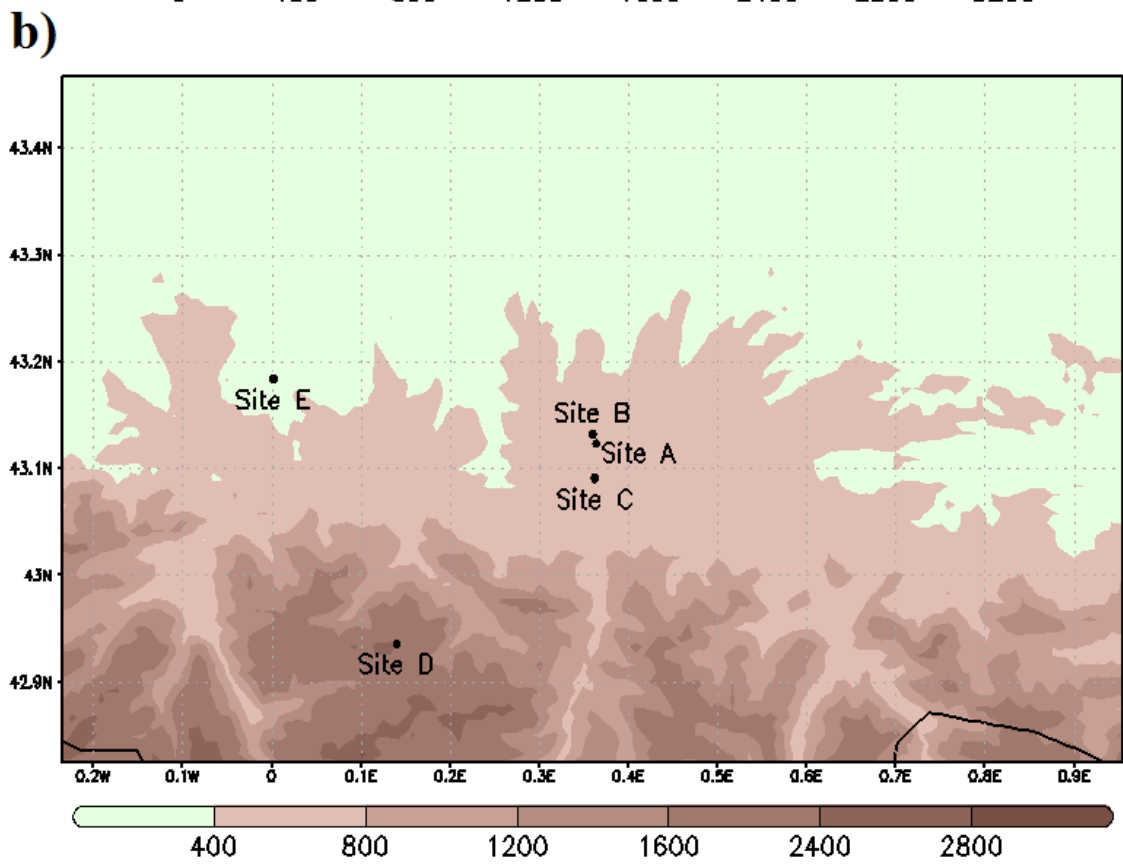
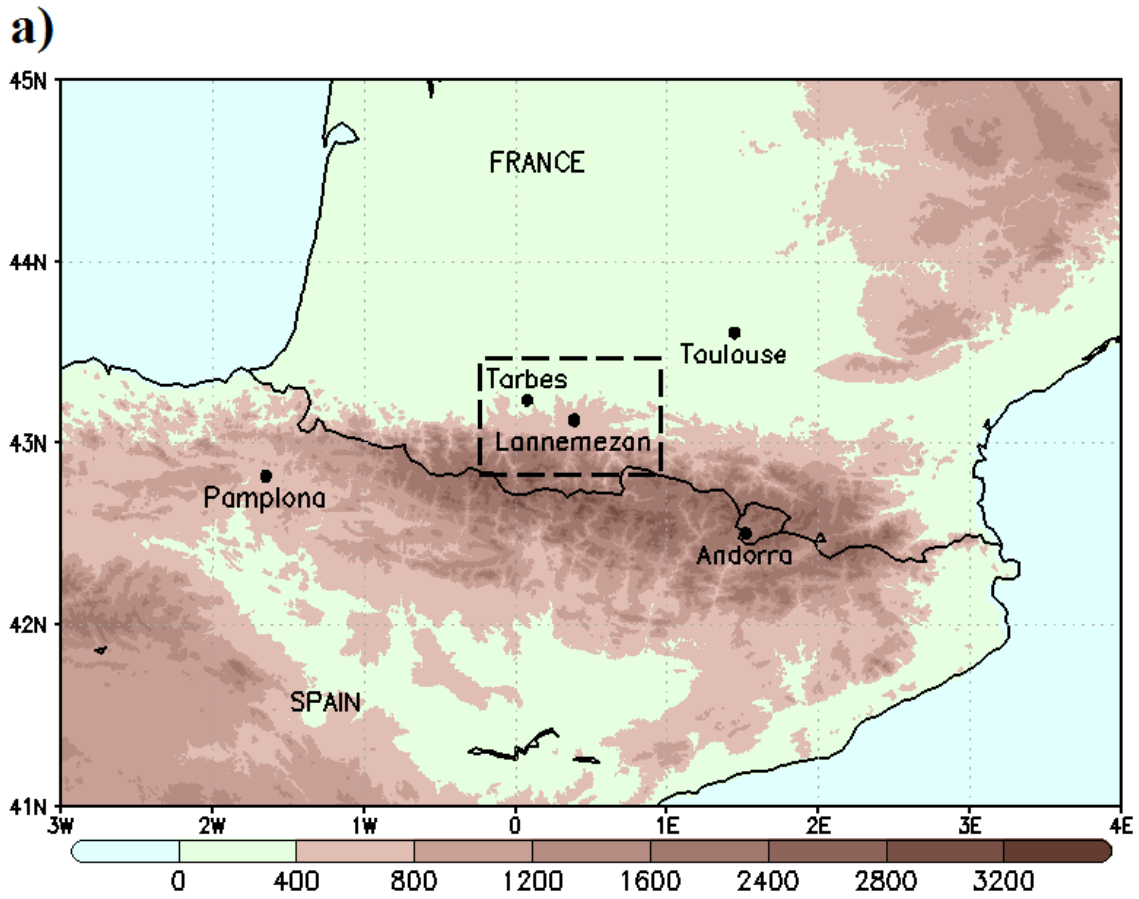


**Figure 1.**

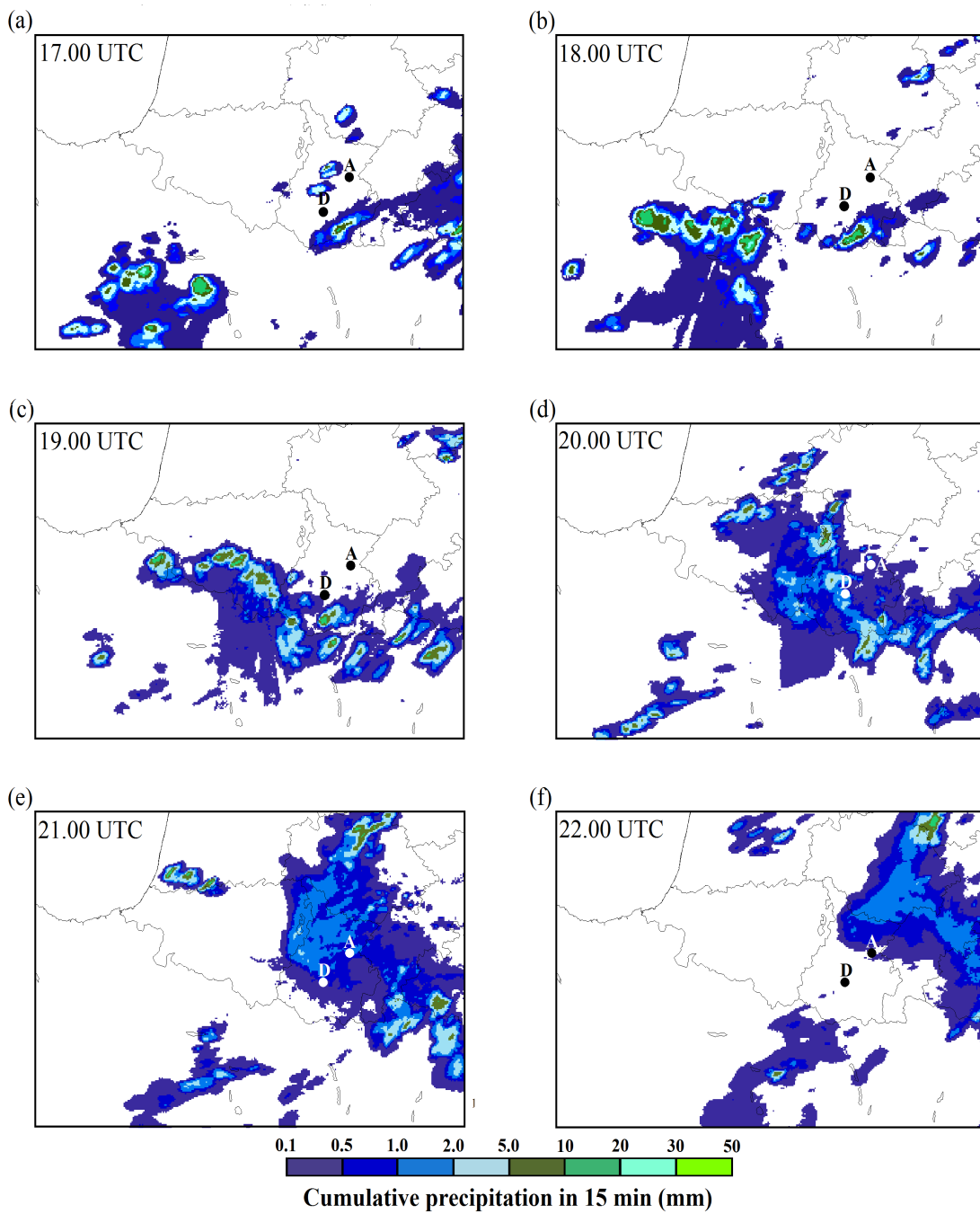
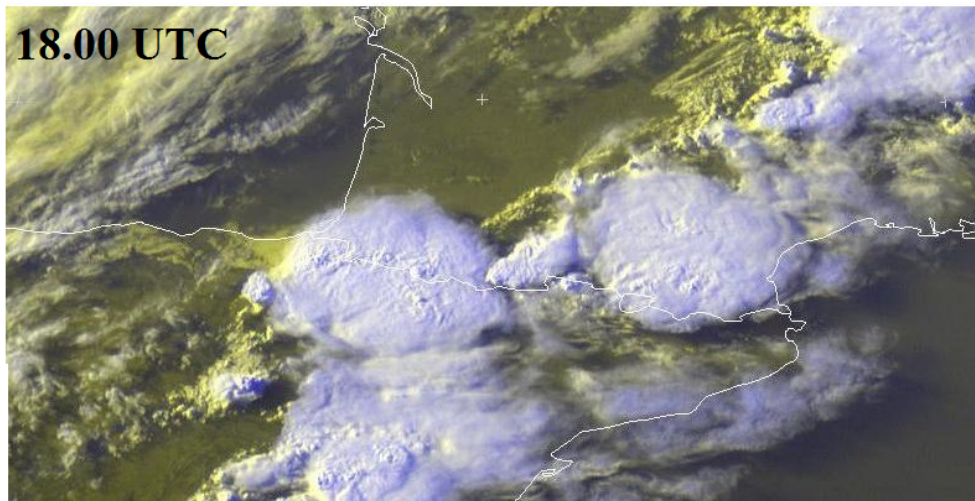
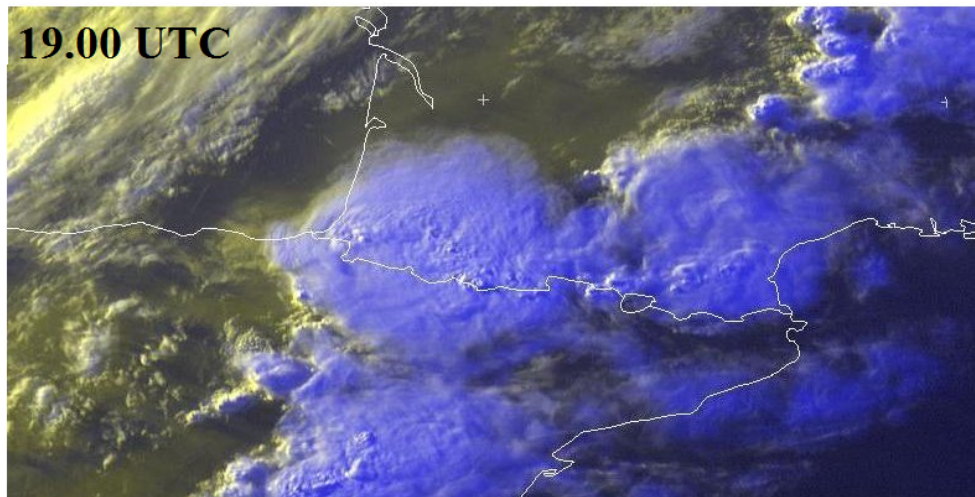


Figure 2.

(a)



(b)



(c)

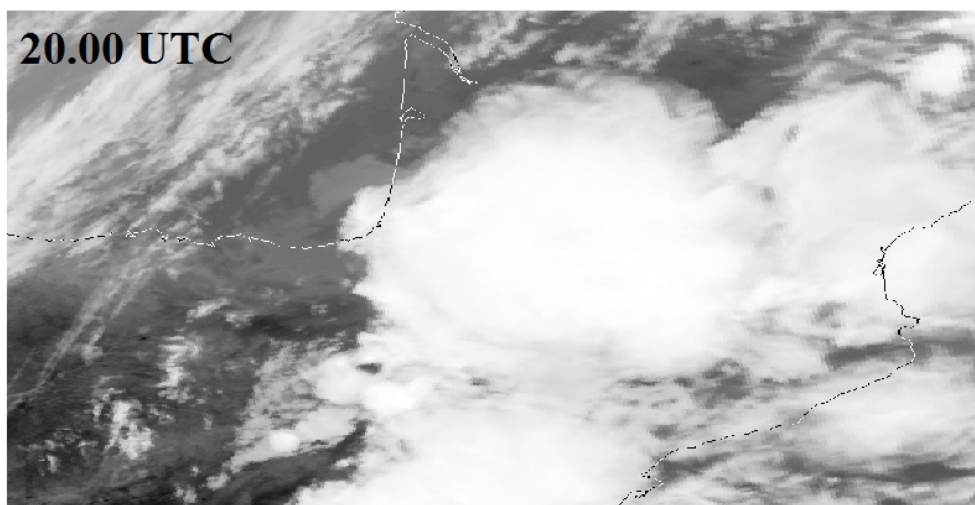


Figure 3.

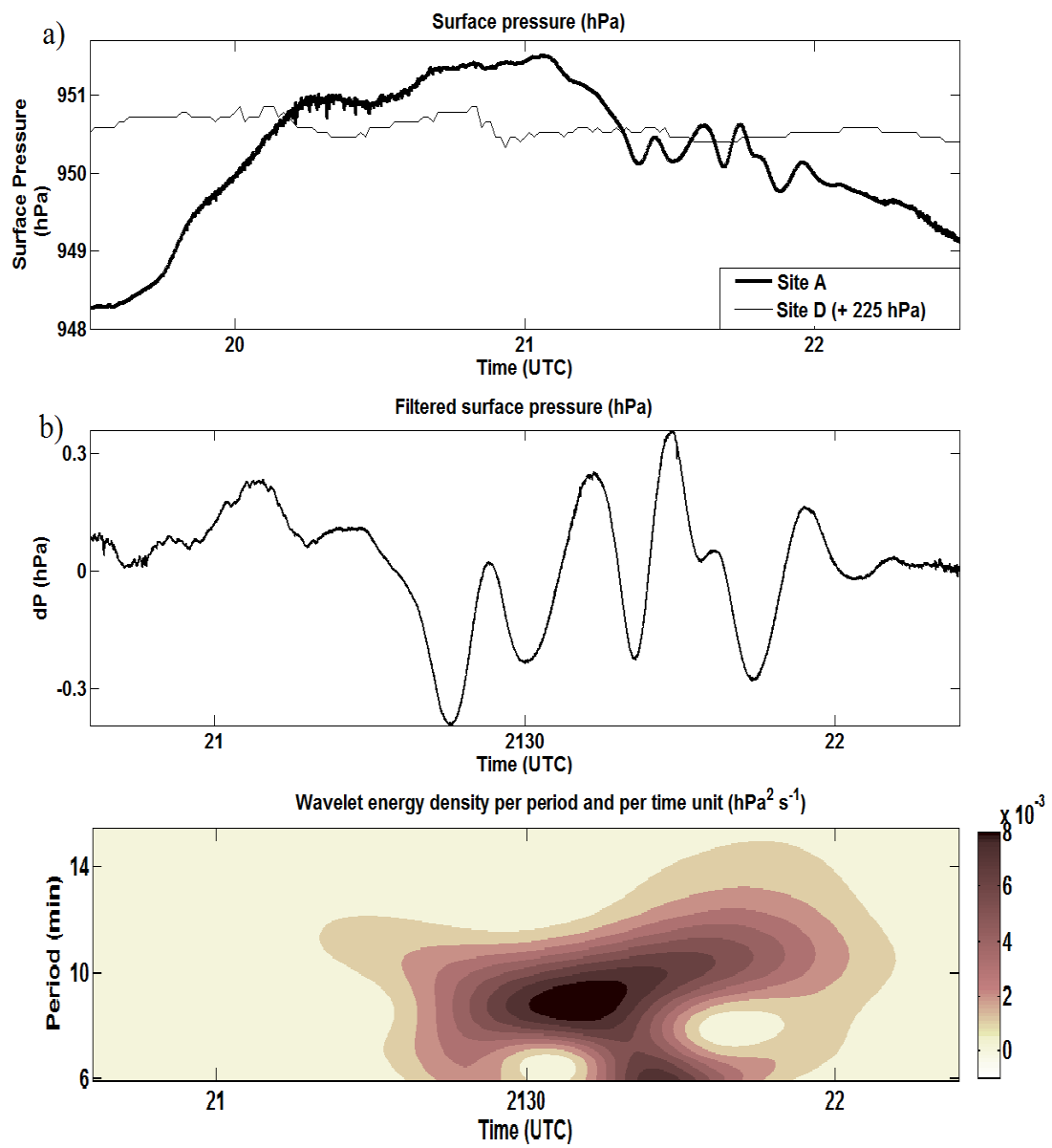


Figure 4.

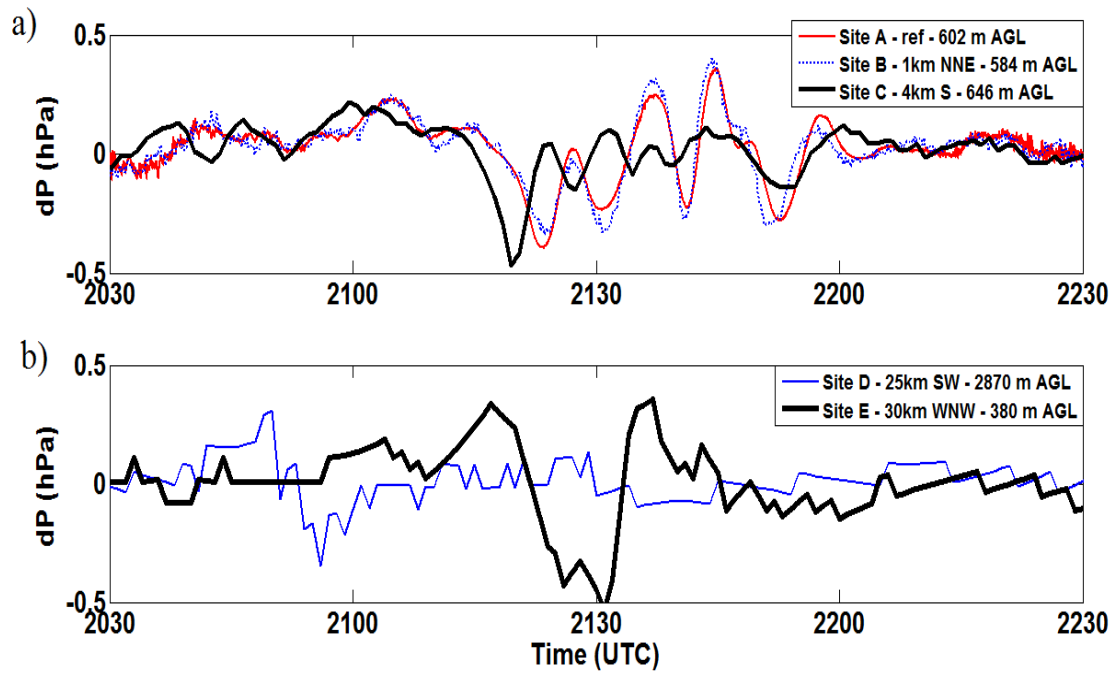


Figure 5.

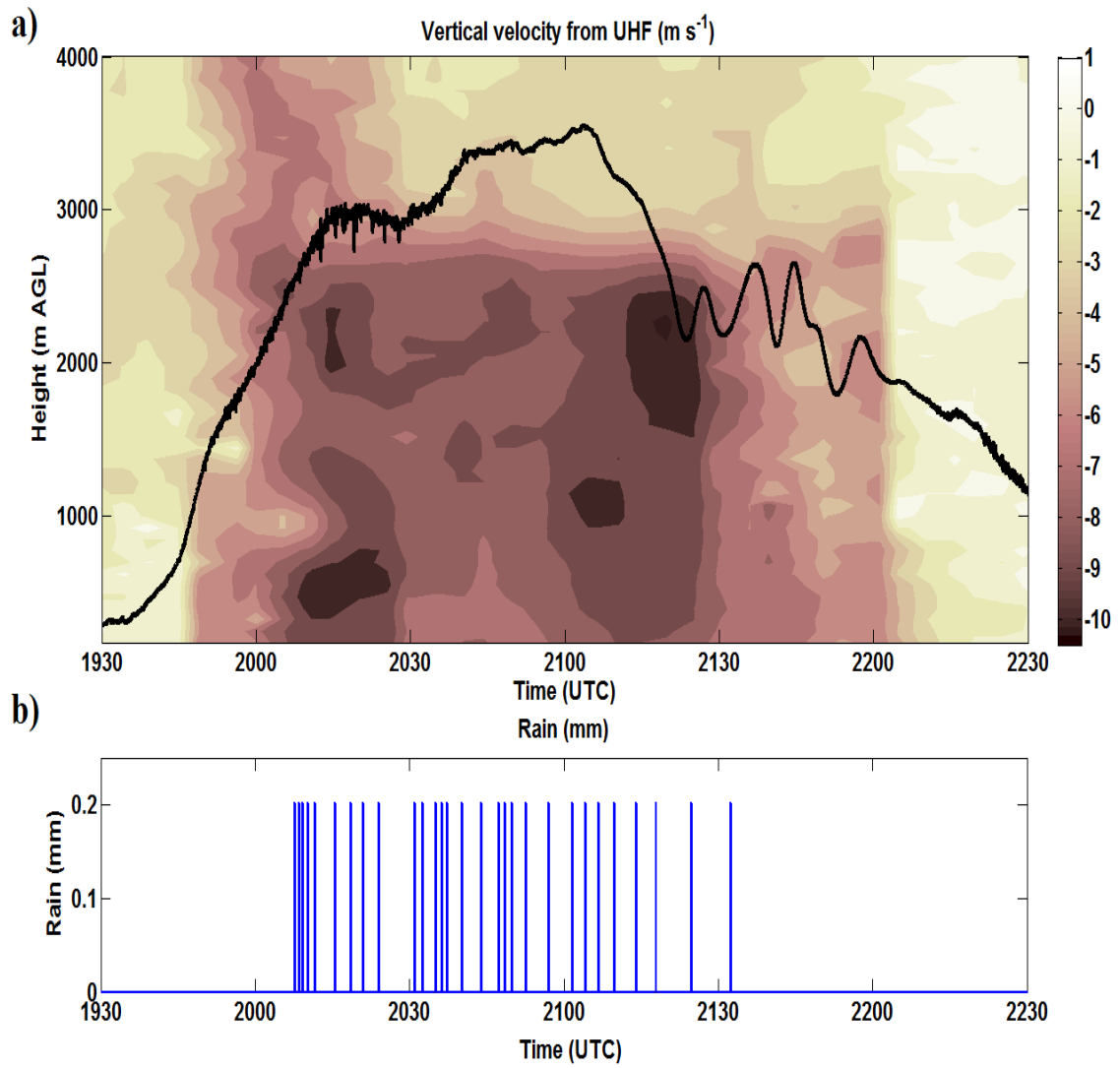
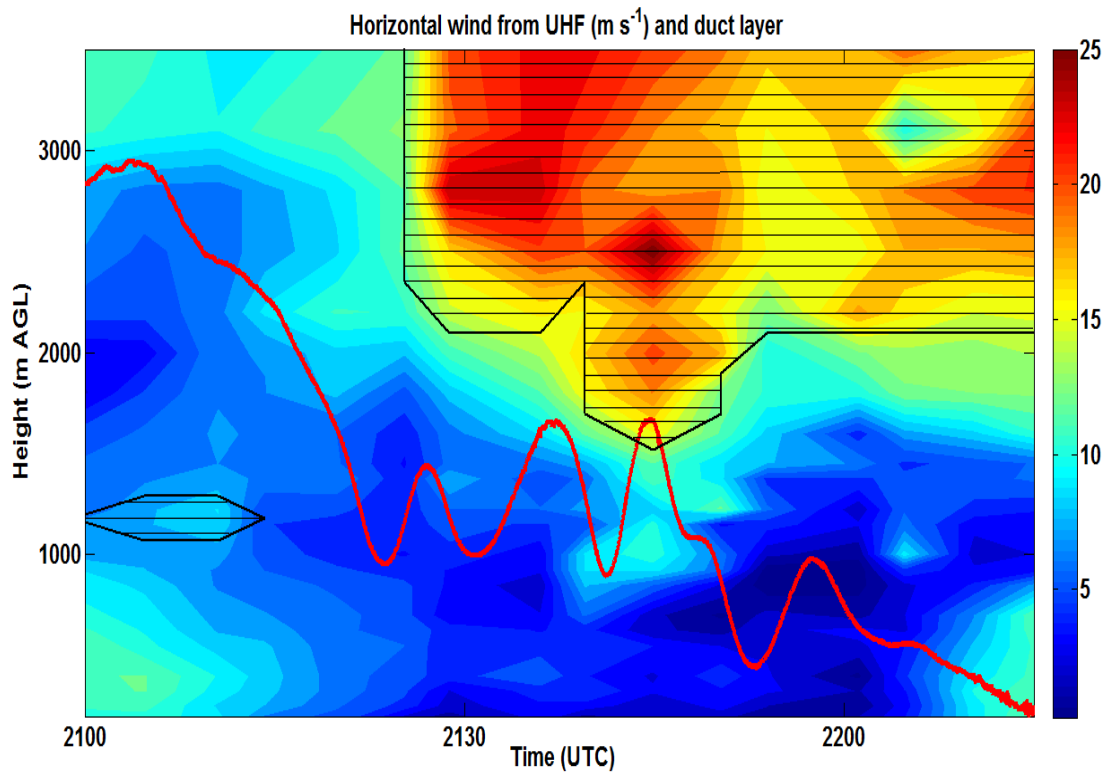
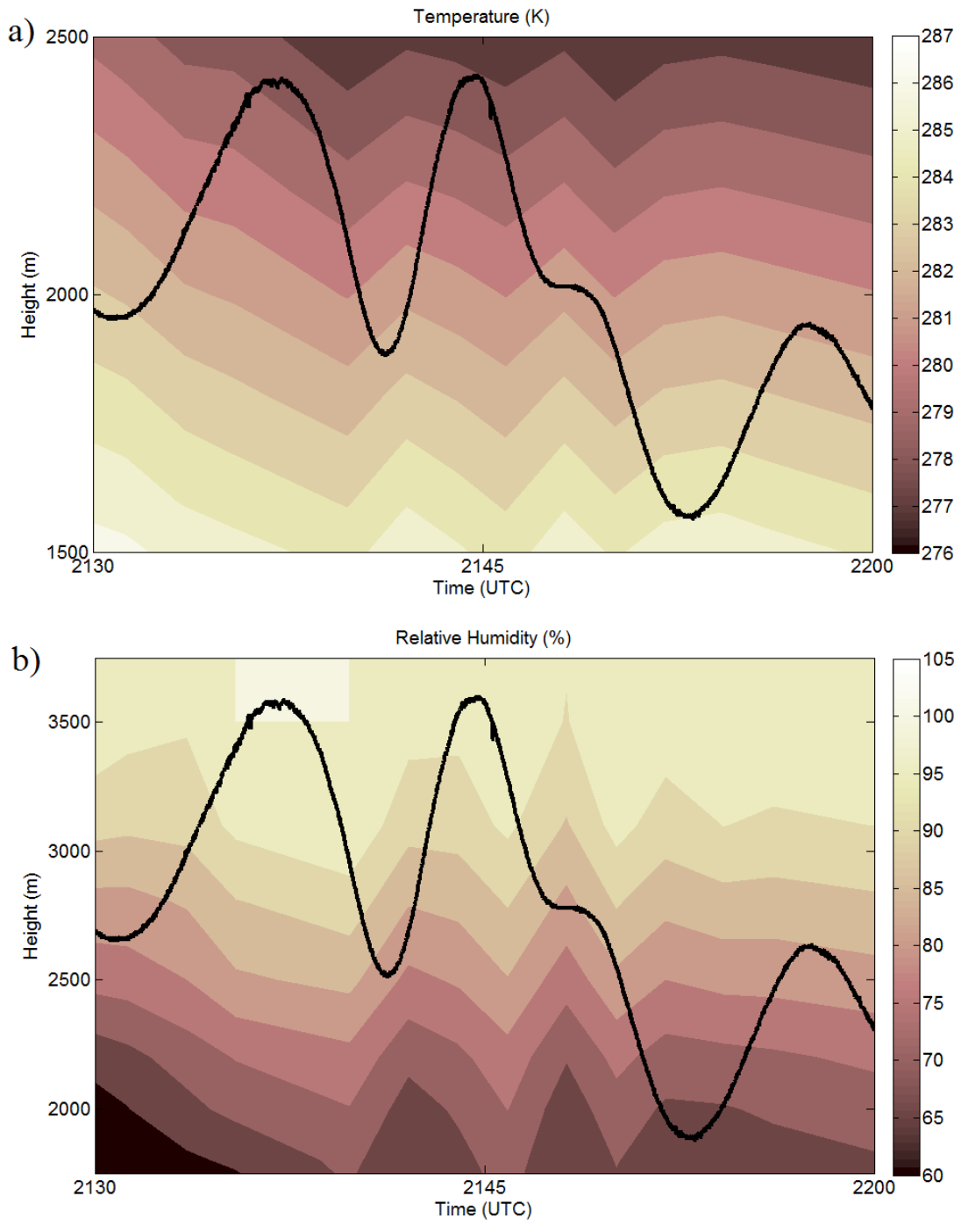


Figure 6.



**Figure 7.**





**Figure 8.**

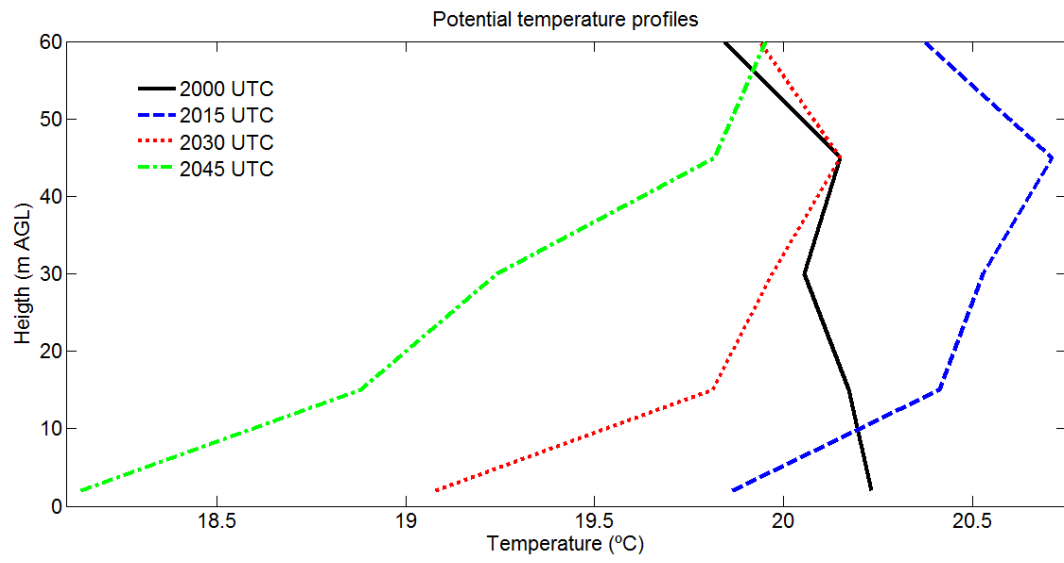


**Figure 9.**

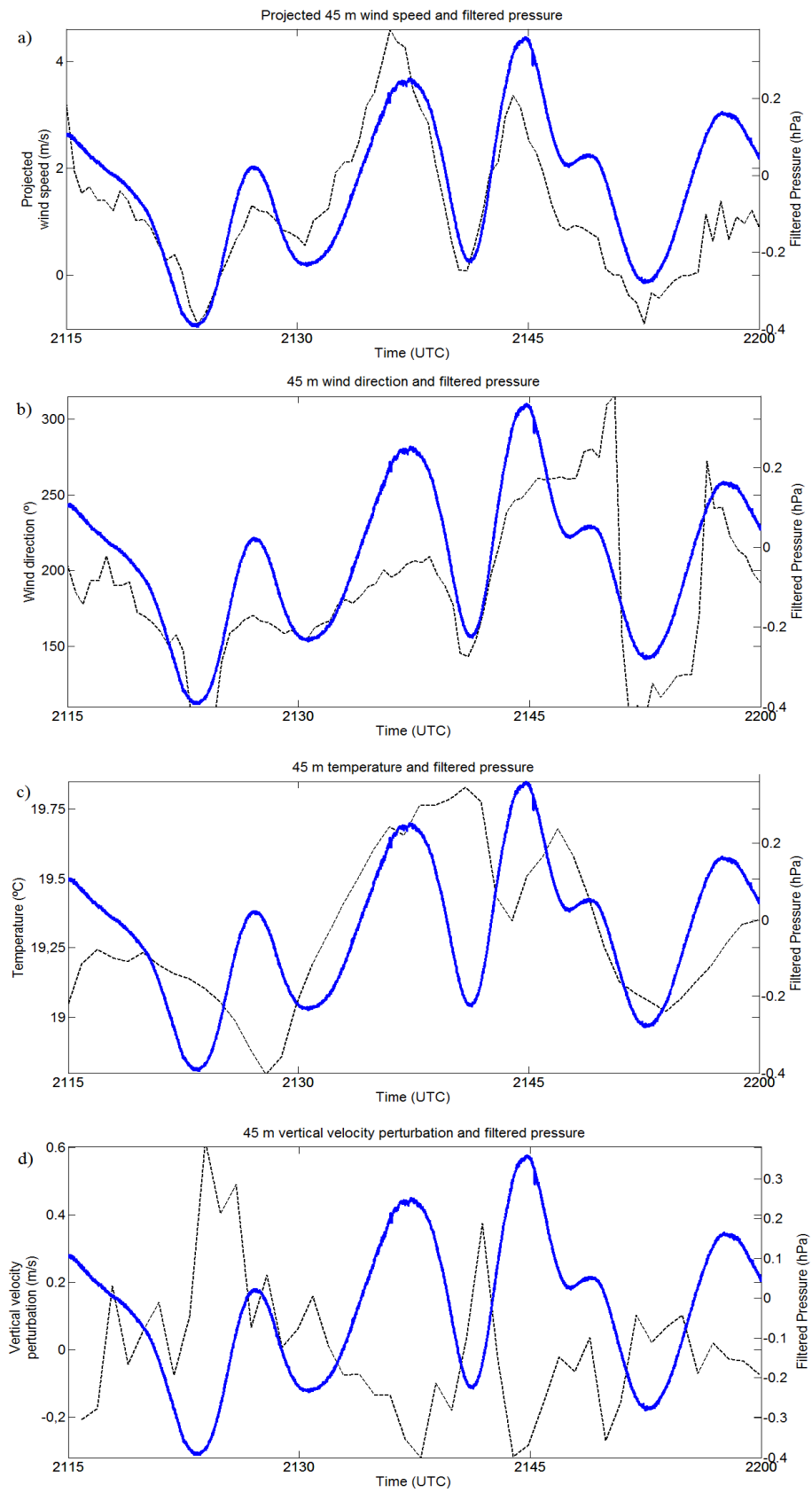


**Figure 10.**

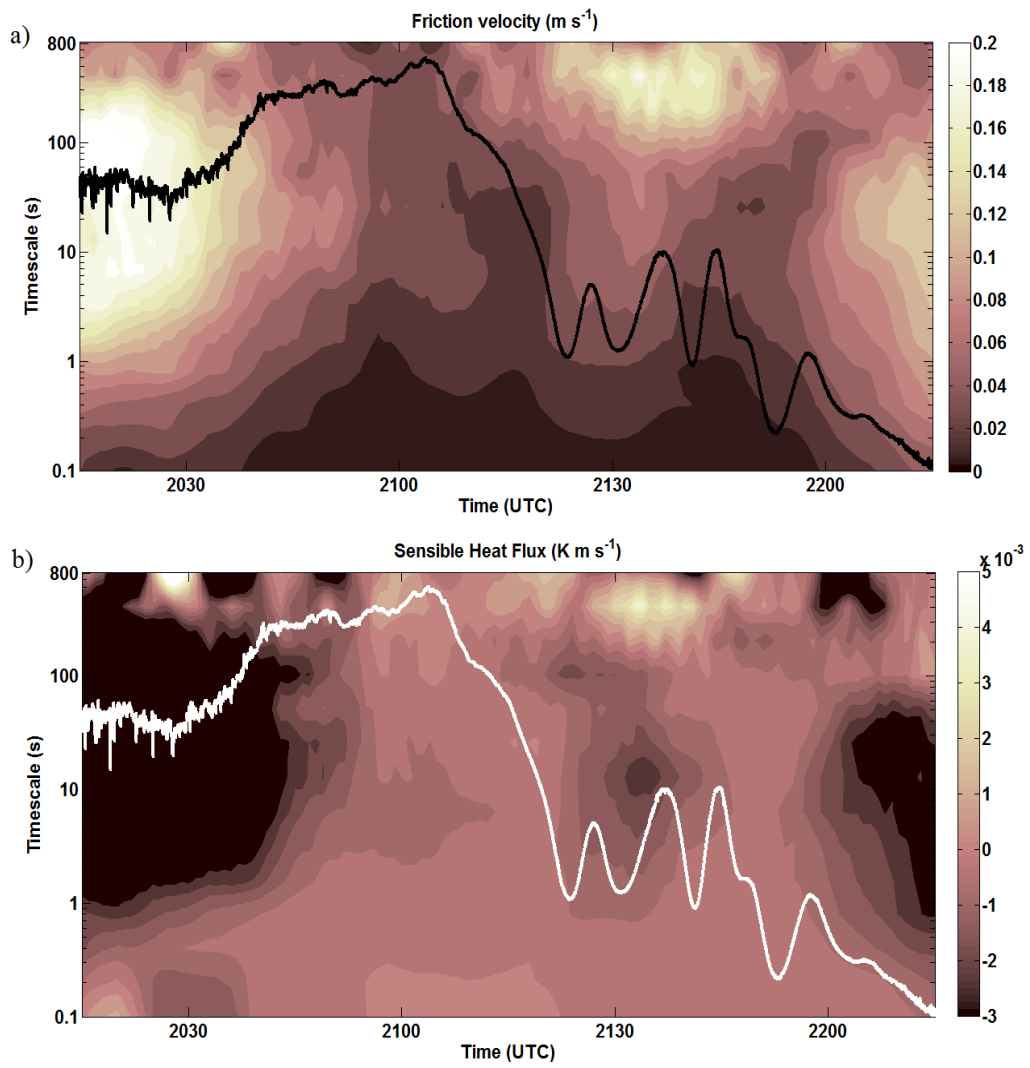


Figure 11.